Emergent relation between surface vapor conductance and relative humidity profiles yields evaporation rates from weather data

Guido D. Salvucci[a,1] and Pierre Gentine[b]

[a]Department of Earth and Environment, Boston University, Boston, MA 02215; and [b]Department of Earth and Environmental Engineering, Columbia University, New York, NY 10027

Edited by Thomas Dunne, University of California, Santa Barbara, CA, and approved March 5, 2013 (received for review September 14, 2012)

The ability to predict terrestrial evapotranspiration (*E*) is limited by the complexity of rate-limiting pathways as water moves through the soil, vegetation (roots, xylem, stomata), canopy air space, and the atmospheric boundary layer. The impossibility of specifying the numerous parameters required to model this process in full spatial detail has necessitated spatially upscaled models that depend on effective parameters such as the surface vapor conductance (C_{surf}). C_{surf} accounts for the biophysical and hydrological effects on diffusion through the soil and vegetation substrate. This approach, however, requires either site-specific calibration of C_{surf} to measured *E*, or further parameterization based on metrics such as leaf area, senescence state, stomatal conductance, soil texture, soil moisture, and water table depth. Here, we show that this key, rate-limiting, parameter can be estimated from an emergent relationship between the diurnal cycle of the relative humidity profile and *E*. The relation is that the vertical variance of the relative humidity profile is less than would occur for increased or decreased evaporation rates, suggesting that land–atmosphere feedback processes minimize this variance. It is found to hold over a wide range of climate conditions (arid–humid) and limiting factors (soil moisture, leaf area, energy). With this relation, estimates of *E* and C_{surf} can be obtained globally from widely available meteorological measurements, many of which have been archived since the early 1900s. In conjunction with precipitation and stream flow, long-term *E* estimates provide insights and empirical constraints on projected accelerations of the hydrologic cycle.

canopy conductance | moisture stress | hydroclimatology

In the simplest terms, evapotranspiration (E) is controlled by the gradient of humidity near the land surface. At the surface, humidity depends strongly on temperature, which itself reflects a balance of radiative heating and cooling, conversion to latent heat, canopy and soil heating, and the turbulent transport of sensible heat into the atmosphere. For a given radiative forcing, the key parameter controlling the relative strength of the turbulent sensible and latent heat fluxes (and thus the magnitude of evapotranspiration) in most land surface models is the surface vapor conductance (C_{surf}) (in meters per second). The surface vapor conductance accounts for the biophysical (e.g., vegetation structure, leaf area, senescence state, stomatal conductance) and hydrological (e.g., soil texture, soil moisture, water table) status of the land surface.

The turbulent fluxes of heat and moisture, however, in turn modify the humidity and temperature of the surface layer, and thus the gradients that drive the fluxes themselves. Given this tight coupling of the surface and boundary layer, one can anticipate statistically meaningful relations to emerge between E and the screen height humidity and temperature, independent of the surface conditions (and thus independent of site-specific model parameters like C_{surf}). This line of reasoning has led to two simplified approaches to estimating E: (*i*) the Priestley–Taylor (1) (*PT*) and Equilibrium (2) evaporation approach, which places constraints on the humidity profile according to the saturation specific humidity (see ref. 3); and (*ii*) the Bouchet–Morton (*BM*) approach (4–8), which, in effect, uses the deviation of atmospheric temperature and humidity from equilibrium conditions to estimate the deviation of E from the equilibrium E rate. The first approach applies to conditions of unlimited moisture supply at the surface (i.e., a wet surface due to moist soil or open water), whereas the latter applies to the more challenging prediction of E from water-limited surfaces. Although intended to be broadly applicable without calibration, the *BM* method is highly sensitive to a dimensionless free parameter that has been found to vary over a wide range (5, 7). Another approach includes so-called extremum (9–11) methods, which are based on maximizing entropy or energy dissipation. These are also justified based on strong atmospheric coupling, but they rely on measurements of the land surface state (e.g., surface skin temperature) instead of screen-height atmospheric measurements.

Here, we propose an approach to estimating E based on a previously undiscovered property of these land–atmosphere interactions. Specifically, heat and moisture fluxes at a set of field sites where E and other meteorological data have been measured reveal an emergent property of the relative humidity (*RH*) profile (the ratio of specific humidity, q, to saturation specific humidity, q^*): the variance of the profile of *RH* in the surface boundary layer is minimized over the course of the day, reflecting a tendency toward thermodynamic equilibration between the land surface and boundary layer. By minimized, we mean that the variance calculated for the same radiative forcing, screen-height temperature, and screen-height specific humidity, but for a too-large surface vapor conductance (C_{surf}) (in meters per second) (and thus larger evaporation flux and smaller sensible heat flux), will always be larger. Likewise, a too small surface vapor conductance (and thus smaller evaporation flux and larger sensible heat flux) will yield a larger variance as well.

Similar to the widely used Penman–Monteith type combination approaches, combining the energy balance constraint with standard diffusion equations alleviates the need for measured surface temperature (12). Unlike the Penman–Monteith approach, however, the need for a priori specification of C_{surf} is also alleviated. Here, C_{surf} is itself estimated by minimizing the predicted variance of the profile *RH*, thereby allowing estimation of evaporation from meteorological data without detailed knowledge of the surface biophysical and hydrological state.

The minimum variance hypothesis is tested by calculating humidity and temperature profiles using the Monin–Obukhov Similarity Theory (with a surface energy balance constraint), while accounting for the additional diffusive transport in the so-called roughness sublayer using a kB^{-1} formulation, and through

Author contributions: G.D.S. designed research; G.D.S. performed research; P.G. contributed new reagents/analytic tools; G.D.S. and P.G. analyzed data; and G.D.S. and P.G. wrote the paper.

The authors declare no conflict of interest.

This article is a PNAS Direct Submission.

[1]To whom correspondence should be addressed. E-mail: gdsalvuc@bu.edu.

the soil and vegetation substrate using an effective surface vapor conductance (12, 13). Varying C_{surf} induces a wide range of E rates, and associated RH profiles, allowing the hypothesis to be tested (see *Methods* for details).

Results and Discussion

The hypothesis is tested at five hydrologically, climatically, and biophysically diverse AmeriFlux (14) sites: Vaira Ranch, a grassland in California; the Duke Forest, a hardwood forest in North Carolina; the Audubon Research Ranch, a desert grassland in Arizona; Fort Peck, a semihumid grassland in the northern great plains of Montana; and Mead Rainfed, an agricultural plot in Nebraska.

Our main finding is that the surface conductance estimated by minimizing the variance of the RH profile predicts the measured E and sensible heat flux accurately. This finding is demonstrated in Fig. 1, where, for each site, three plots are presented: (*i*) the mean seasonal cycle of predicted and measured latent heat flux (i.e., the energy equivalent of evapotranspiration), filtered with an 11-d moving window average (Fig. 1 *A*, *D*, *G*, *J*, and *M*); (*ii*) a single year or season of results highlighting the covariability of the measured and estimated daily averaged fluxes (Fig. 1 *B*, *E*, *H*, *K*, and *N*); and (*iii*) a scatter plot of the daily-estimated and measured fluxes, along with a root mean square and mean bias estimate (Fig. 1 *C*, *F*, *I*, *L*, and *O*).

The fit between the measured (green) and estimated (red) fluxes, at both seasonal and synoptic scales, across five significantly different field sites, corroborates the hypothesis that the RH profile evolves to a minimum variability with respect to evaporation. Note again that the estimated surface vapor conductances (and corresponding evaporation rates) were not calibrated with the observed evaporation rates. C_{surf} was estimated only from the RH profiles, the calculation of which was based only upon measured humidity, temperature, ground heat flux, friction velocity (or wind speed), net shortwave radiation, and incoming longwave radiation.

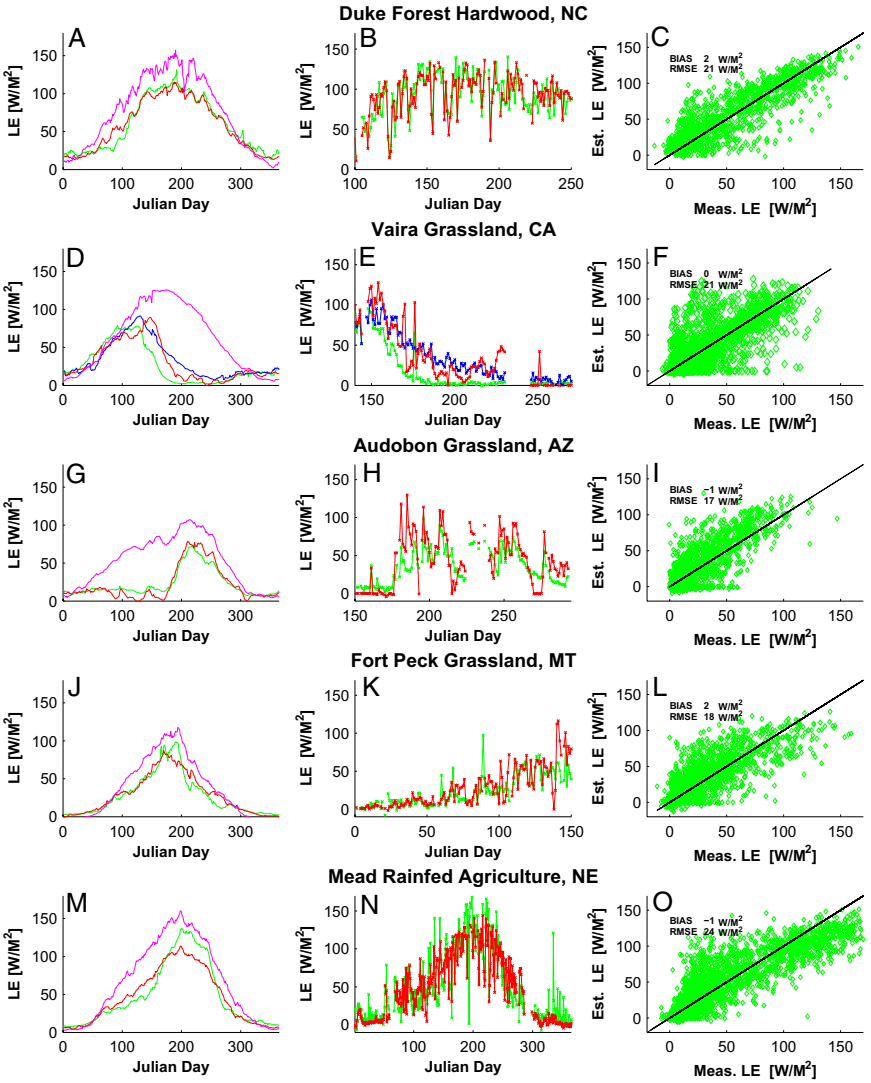

Fig. 1. Estimated and measured latent heat fluxes at five AmeriFlux test sites. The first column (*A*, *D*, *G*, *J*, and *M*) contains climatological means, highlighting seasonal water limitations, the second column (*B*, *E*, *H*, *K*, and *N*) contains selected periods highlighting synoptic variations, and the third column (*C*, *F*, *I*, *L*, and *O*) contains a scatter plot of the daily measured and predicted values, along with statistics of fit. The green lines are measured fluxes, the red lines are predicted fluxes based on minimizing the *RH* profile variance, and the magenta lines are the Priestley–Taylor (water-unlimited) estimates for reference. In *D* and *E*, the blue lines are measured fluxes at Tower B (see text for detail). The highlighted seasons in *B*, *E*, *H*, *K*, and *N* are for years 2007, 2010, 2005, 2007, and 2009, respectively.

The ability to use this emergent property of the coupled land–atmosphere system as a means to estimate evaporation is particularly dramatic at the Vaira Ranch site, which undergoes a major seasonal dry down in the summer (Fig. 1 *D–F*) and at the Audubon Research Ranch site, which undergoes a major wetting-up (and greening-up) period with summer rains (Fig. 1 *G–I*). At the same time, the methodology does not overestimate evaporation at the more humid sites with more temporally consistent moisture supply (Fig. 1 *A–C*, *J–L*, and *M–O*). At these sites, both the measured (green lines) and estimated (red lines) evaporation rates correlate well with the simple Priestly–Taylor model (magenta lines), indicating that net radiation is the dominant limiting factor. Priestly–Taylor is used here to give a rough sense of energy limitations, and its parameter has been held at 1.26 and not calibrated to each site. Note that, in Fig. 1 *D* and *E*, the green lines labeled Tower A plot *LE* measured at the Vaira Ranch (grassland) site, whereas the blue lines labeled Tower B plot *LE* from the nearby (~3 km away) Tonzi Ranch (woody savannah) site. The predictions (red lines) based on *RH* calculated from Tower A measurements are roughly bounded by the two tower values (Fig. 1*D*) and are well correlated with the average of the two tower values (Fig. 1*F*). This could be interpreted as an overestimation by the proposed method, or as an indication that the method reflects energy balance partitioning over a larger footprint than the eddy covariance method measures. The latter interpretation is consistent with a recent finding (15) that scalars are a wider integrator of landscape variability. This case also highlights the difficulty that the proposed method, like others based on land–atmosphere interactions (1–8), face in patchy landscapes where assumptions of statistical homogeneity of the boundary layer may be violated.

Finally, although the overall bias of the daily-averaged *LE* is small in all five test cases, there does appear to be some magnitude-dependent structure to the error, such that the estimation procedure underestimates *LE* when *LE* is large, and overestimates it when it is small. This is most apparent in the Mead Rainfed Agricultural site in both the seasonal cycle (Fig. 1*M*) and in the scatter plot (Fig. 1*O*), but also appears, to a lesser degree, in the other cases.

The observed minimization of *RH* variance is most likely a rapid response of the boundary layer temperature and humidity to more slowly varying (largely soil moisture and leaf area-dependent) surface conductance, as opposed to a response of the surface conductance to the atmosphere. In other words, we interpret the "selected" surface conductance parameter as being the value most likely to have yielded the observed air temperature and humidity. Feedbacks that could yield the observed minimization of *RH* variance are being explored in coupled diffusion and radiative transfer models.

In the tests presented in Fig. 1, all required measurements were available. For applications outside of experimental field sites [e.g., using historical weather station data to estimate long term hydroclimatic trends (16) and evaluate climate model projections (17)], ground heat flux, incoming longwave radiation, and, in some cases shortwave radiation data, will not be available. For these applications, semiempirical relations (13, 18) will need to be used to estimate these terms from the measured variables [e.g., incoming longwave radiation can be estimated (19) from screen height temperature and humidity]. Outside of experimental sites, u_* is not typically available, but it can be estimated from wind speed using the Businger–Dyer momentum stability functions (13, 18).

By applying the minimum variance of *RH* property, along with the aforementioned semiempirical estimates of any unavailable meteorological measurements, robust estimates of E and C_{surf} can be obtained globally. By relying mostly on basic weather data, such estimates will have far greater spatial coverage than the direct measurements available at experimental sites (e.g., ref. 14) and will have temporal coverage extending, in some areas, to the early 1900s. In conjunction with existing hydrologic and climatic records, such global, long-term E estimates could provide insights and empirical constraints on climate model projected accelerations of the hydrologic cycle.

Methods

Land–Atmosphere System Equations. Monin–Obukhov similarity theory is used, in conjunction with surface energy balance and the Businger–Dyer stability functions, to describe the land–atmosphere system (13, 18) and estimate *RH* profiles for a range of values of C_{surf}. In summary, the profiles of potential temperature (θ) and specific humidity (q): (*i*) pass through observed screen-height temperature and humidity for observed values of the friction velocity (u^*) (in meters per second); (*ii*) account for water vapor diffusion through the soil and vegetation substrate using a daily-constant surface conductance (C_{surf}); and (*iii*) yield fluxes that are in balance with measured net shortwave and incoming longwave radiation, modeled outgoing longwave radiation, and measured ground heat flux. In this framework, each value assumed for C_{surf} yields a unique diurnal cycle of surface temperature, turbulent fluxes, and relative humidity profiles. Equations describing this system follow.

The specific humidity (q) (kilogram/kilogram) profile is described by the following:

$$q = q_s - \left(\frac{E}{k u_* \rho}\right)\left[\ln\left(\frac{z-d}{z_{ov}}\right) - \Psi_v\left(\frac{z-d}{L}\right) + \Psi_v\left(\frac{z_{ov}}{L}\right)\right]. \quad [1]$$

In Eq. **1**, E is the evapotranspiration mass flux (in kilograms per meter^2 per second), k is the dimensionless von Karman constant, set to 0.41, ρ is air density (in kilograms per meter^3), u_* is the friction velocity (in meters per second), z is height above the surface (in meters), d is the displacement height, set to 0.7 times the vegetation height (z_{veg}), L is the Obukhov length (in meters), and z_{ov} is the roughness length (in meters) for water vapor. The subscript s denotes surface values (e.g., q_s is the surface humidity), where the surface is defined as the roughness height plus the displacement height (e.g., $d + z_{ov}$). Ψ_v in Eq. **1** is the stability function for water vapor, which describes the deviation of the specific humidity profile from the standard logarithmic (law of the wall) profile due to either stabilizing or destabilizing thermal stratification. The Obhukov length (L) is given by the following:

$$L = \frac{-u_*^3 \rho \theta_a \cdot (1 + \epsilon q_a) \cdot c_p}{kg \cdot (H + c_p \theta_a \epsilon E)}. \quad [2]$$

In Eq. **2**, c_p is the specific heat of air at constant pressure (1,004 J·kg^{-1}·°C^{-1}), g is the gravitational acceleration (9.81 m·s^{-2}), R_v is the gas constant for water vapor (461 J·kg^{-1}·°C^{-1}), ϵ is the dimensionless ratio of the gas constant for dry air (R_d, 287 J·kg^{-1}·°C^{-1}) to water vapor, which is 0.622, H is the sensible heat flux (in joules per meter^2 per second^{-1}), and q_a and θ_a are the specific humidity and potential temperature at the measurement height.

The potential temperature (θ) profile is of similar form to q:

$$\theta = \theta_s - \left(\frac{H}{k u_* \rho c_p}\right)\left[\ln\left(\frac{z-d}{z_{oh}}\right) - \Psi_h\left(\frac{z-d}{L}\right) + \Psi_h\left(\frac{z_{oh}}{L}\right)\right]. \quad [3]$$

In Eq. **3**, z_{oh} is the roughness length (in meters) for heat.

The stability functions used for vapor and heat are given in terms of dimensionless height ξ as follows (13, 18):

$$\Psi_h = \Psi_v = \begin{cases} 2\ln[(1+\mathrm{sqrt}(1-16\xi))/2] & \xi < 0 \\ -5\xi & 0 \le \xi \le 1 \\ -5 - 5\ln(\xi) & \xi > 1. \end{cases} \quad [4]$$

The roughness heights for water vapor and heat are estimated using the so-called kB^{-1} approach (13, 20) relating the momentum (z_o) and scalar (z_{oh} and z_{ov}) roughness heights to the roughness Reynolds number R_{e^*} as follows:

$$kB^{-1} = \ln\left(z_o/z_{ov}\right) = \ln\left(z_o/z_{oh}\right) \simeq k \cdot \left(6R_{e^*}^{\frac{1}{4}} - 5\right). \quad [5]$$

In Eq. **5**, the roughness Reynolds is defined as $u_* z_o/\nu$, where ν is the kinematic viscosity, taken as 1.45E-5 m^2·s^{-1}. In refs. 13 and 20, the factor multiplying R_{e^*} in Eq. **5** is given as 6.2 for heat and 5.7 for water vapor. Here we have expressed both as 6. The momentum roughness (z_o) is set to 0.1 times the vegetation height (z_{veg}).

The evapotranspiration mass flux (E) in Eq. **1** is related to the latent heat flux (LE), plotted in Fig. 1, through the following:

$$LE = \lambda E. \quad [6]$$

In Eq. **6**, λ is the latent heat of vaporization (taken as 2.502E6 J·kg^{-1}). The energy balance of the land surface is written as follows:

$$R_{sd} - R_{su} + R_{ld} - R_{lu} - LE - H - G = 0. \quad [7]$$

In Eq. **7**, R_{sd} is the measured solar downwelling radiation, R_{su} is the measured upwelling (reflected) solar radiation, R_{ld} is the measured longwave downwelling radiation, H and LE are the turbulent fluxes of sensible heat and latent heat, and G is the measured ground heat flux, all given in joules per meter^2 per second.

The upwelling longwave flux (R_{lu}) is modeled based on surface temperature (T_s), the Stefan–Boltzmann constant (σ), and emissivity (ε), taken here as 0.99, as follows:

$$R_{lu} = \varepsilon \sigma T_s^4. \quad [8]$$

Specific humidity (q) is related to the partial pressure of water vapor (e) through the following:

$$q = \frac{\epsilon e}{P - (1-\epsilon)e}. \quad [9]$$

In Eq. **9**, P is atmospheric pressure (in newtons per meter^2), whose vertical variation is modeled using an isothermal and hydrostatic approximation as follows:

$$P = P_s \cdot \exp\left(\frac{-gz}{R_d T_{ref}}\right). \quad [10]$$

In Eq. **10**, P_s is the measured surface pressure.

Saturation specific humidity (q^*) is related to saturation vapor pressure (e^*) using Eqs. **9** and **10**, and the integrated Clausius–Clapeyron relation, approximated here from Garratt (13) as follows:

$$e^* = 611.2 \cdot \exp\left(\frac{17.67 \cdot (T - 273.15)}{T - 29.65}\right). \quad [11]$$

The potential (θ) and actual (T) temperatures are related using the definition of potential temperature and the modeled hydrostatic pressure distribution (Eq. **10**):

$$T = \theta \cdot \left(\frac{P}{P_s}\right)^{R_d/c_p} \cong \theta \cdot \exp\left(\frac{-gz}{R_d T_{ref}}\right)^{R_d/c_p}. \quad [12]$$

The final equation required in this framework is one expressing the additional limitation on evaporation as water vapor diffuses from the sites of evaporation (e.g., soil pores, stomatal cavities), at which location q is saturated at the temperature T_s (i.e., where $q = q^*(T_s)$), to the free air at the nominal surface level ($d + z_{ov}$), i.e., where we denote q by q_s. This limitation is modeled with a single surface conductance parameter C_{surf} (m s^{-1}) as follows:

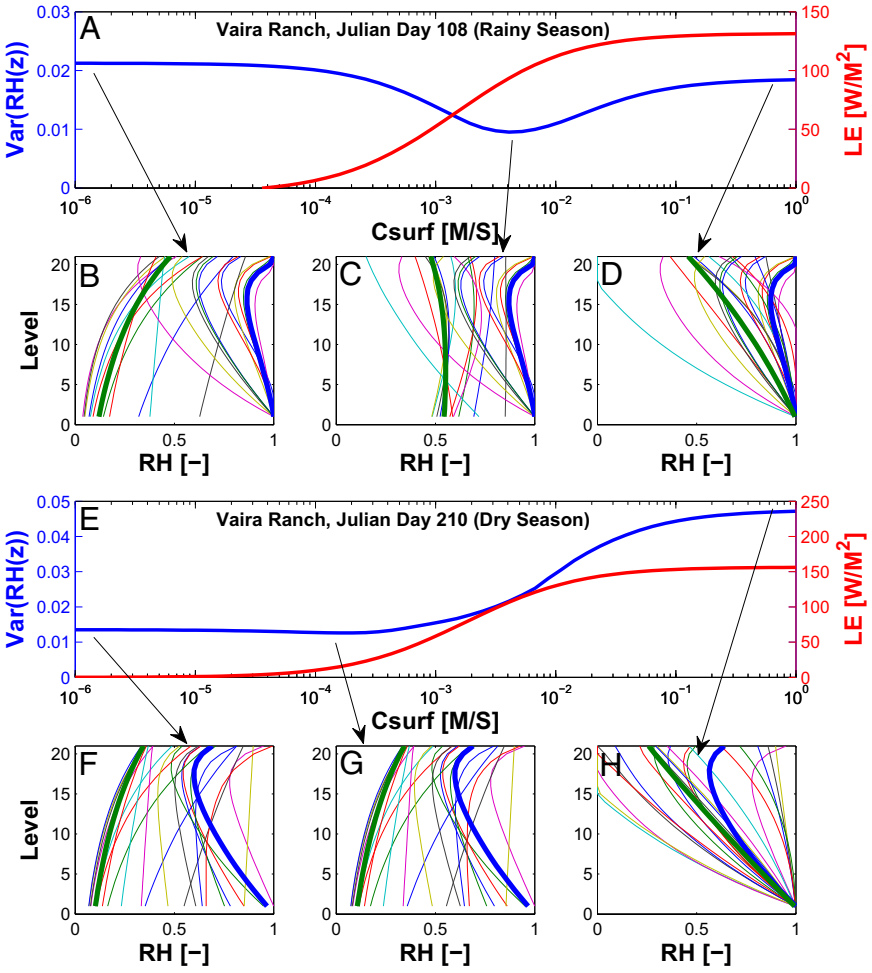

Fig. 2. Demonstration of minimization of *RH* profile variance at the Vaira Ranch site. The first and third rows (*A* and *E*) plot the daily-averaged vertical *RH* profile variance (blue line) and the daily averaged latent heat flux (LE) (red line) as a function of C_{surf}, for an energy-limited day (*A*) and a moisture-limited day (*E*). The second and fourth rows (*B*, *C*, *D*, *F*, *G*, and *H*) display diurnal relative humidity profiles plotted against the model level (i.e., increment of the nondimensional distance $\zeta = \left[\ln\left(\frac{z-d}{z_{oh}}\right) - \Psi_h\left(\frac{z-d}{L}\right) + \Psi_h\left(\frac{z_{oh}}{L}\right)\right]$) for the three values of C_{surf} indicated by the downward pointing arrows. Profiles at 3:00 AM and 3:00 PM are highlighted in thick blue and thick green lines, respectively, to emphasize the diurnal cycle.

$$E = \rho \cdot C_{surf} \cdot \left(q^*(T_s) - q_s \right). \quad [13]$$

Eq. **13** links the surface energy balance to the specific humidity profile (Eq. **1**) through their mutual dependence on q_s.

Note that through Eqs. **6** and **9–13**, the latent heat flux (*LE*) appearing in the energy balance equation (Eq. **7**) becomes dependent on surface temperature, coupling the system of equations. With a measurement of u_*, R_{sd}, R_{su}, R_{sld}, and G, along with θ and q at some measurement height z, Eqs. **1–13** are solved for simultaneously (via iteration) for surface temperature and for the associated fluxes of latent and sensible heat. If condensation is predicted for large C_{surf} (e.g., at night), C_{surf} is set to the largest value for those half-hour increments (because condensation onto surfaces does not encounter stomatal or soil resistance).

Calculation of Vertical Variance of RH Profile and Estimation of C_{surf}. The *RH* profile is then calculated from Eqs. **1–3** and **9–12**. The vertical variance of the *RH* profile is calculated with *RH* evaluated at 20 evenly spaced values of the nondimensional distance $\zeta = \left[\ln\left(\frac{z-d}{z_{oh}}\right) - \Psi_h\left(\frac{z-d}{L}\right) + \Psi_h\left(\frac{z_{oh}}{L}\right) \right]$ from source height ($z = z_{oh} + d$), where $\zeta = 0$, to the boundary layer top ($z = Z_{top}$, set to 1,000 m). Z_{top} can range from 250 to 1,000 m with little impact on predicted *E*. Note that from the linear diffusion equation form of Eqs. **1** and **3**, these increments of space can be interpreted, heuristically, as mixing lengths. Plotted in this nondimensional, scaled ζ space, θ and q vary linearly (as a passive scalar would plot against distance at steady-state molecular diffusion). Note, however, that the *RH* profiles are not linear, due to **Eqs. 11** and **12**. The *RH* profile and its vertical variance are calculated at each of the 48 half-hourly increments resolved by the AmeriFlux data. The 48 half-hourly vertical variances are then time averaged to a single, daily-average vertical variance. The calculations are performed numerically, as the nonlinearities present in the equation do not lend themselves to an analytic expression for the variance.

An example of the estimation procedure is illustrated in Fig. 2 for an energy-limited day (Julian day 108) and moisture-limited day (Julian day 210) at the Vaira Ranch site. The top row (Fig. 2*A*) and third row (Fig. 2*E*) show the daily-averaged vertical variance of relative humidity (blue lines) as a function of the surface vapor conductance C_{surf}. Note the distinct, symmetrical minimum in the variance during the wet season, and the less distinct and asymmetrical minimum in the dry season. Fig. 2 *A* and *E* also show the daily averaged latent heat flux (*LE*) in red lines with values corresponding to the second vertical axis (to right of figure). Although the ability to distinguish small values of C_{surf} during the drydown is clearly compromised by the relative lack of concavity of the variance, note that, for these values, *LE* itself is relatively insensitive to C_{surf}, such that estimation of *LE* remains robust. Also note that the concavity of the variance at the minimum value is controlled by the sensitivity of *LE* to C_{surf}. For example, if the minimum occurs at a C_{surf} for which *LE* is already close to zero (as in Fig. 2*E*), concavity is small, whereas if it occurs at moderate values of *LE* for which *LE* is still sensitive to C_{surf}, the concavity is large (Fig. 2*A*). In the dry case (Fig. 2*E*), lowering C_{surf} beyond 10^{-4} m·s^{-1} has little impact on *LE,* as most of the incoming energy is partitioned to *H*, *G*, and R_{lu}, and thus the profiles of *RH* are changed only slightly (e.g., compare Fig. 2 *F* and *G*).

The second row (Fig. 2 *B–D*) and fourth row (Fig. 2 *F–H*) display diurnal relative humidity profiles plotted against the model level (i.e., increment of the nondimensional distance $\zeta = \left[\ln\left(\frac{z-d}{z_{oh}}\right) - \Psi_h\left(\frac{z-d}{L}\right) + \Psi_h\left(\frac{z_{oh}}{L}\right) \right]$). For each case, the three sets of profiles correspond to calculations made with a too-small C_{surf} , the C_{surf} that minimizes the variance, and a too-large C_{surf}. For both days, the middle case (the chosen value) can be seen to have the most vertically constant *RH* profiles. The profiles corresponding to 3:00 AM and 3:00 PM are highlighted in thick blue and thick green lines, respectively, to emphasize the diurnal cyle.

The sensitivity of the *RH* profiles (calculated from the governing diffusion and energy balance Eqs. **1–13**) to the surface vapor conductance is evident. Large values of C_{surf} (e.g., Fig. 2*D*) lead to large latent heat (*LE*) fluxes and small sensible heat (*H*) fluxes, consistent with large surface specific humidity (q_s), low temperature at the surface, and thus large *RH* at the surface. Conversely, very small C_{surf} greatly reduces the *LE* and increases sensible *H*. Under these conditions, there is little humidity gradient (q_s is approximately equal to that at measurement height), whereas a strong temperature gradient exists to maintain *H*. The *RH* thus increases with height away from the surface, as the saturation humidity (q^*) decreases with decreasing temperature.

To improve the robustness of the minimization with respect to synoptic scale variability of the meteorological forcing data, we then further window average the daily-averaged variance of the *RH* profile before estimating C_{surf} . Because daily variations of C_{surf} are regulated mainly by soil moisture and leaf area index, each of which show significant variability at timescales on the order of weeks to months, the length of the window is set to the minimum of 21 d or the length of time without precipitation. In this way, estimates of C_{surf} vary smoothly, except when rainfall rapidly increases soil moisture.

Notes on AmeriFlux Data. The data used in the analysis are all available as the so-called "Level 2 with gaps" files at the AmeriFlux data repository (14). The only adjustments made to these data were as follows: (*i*) If the measured energy balance (net radiation minus latent, sensible, and ground heat flux) at any half-hourly measurement exceeds 300 J·m^{-2}·s^{-1}, the fluxes for that half hour were treated as missing; (*ii*) if the measured energy imbalance summed over the day exceeded 50 J·m^{-2}·s^{-1}, the whole day was excluded from the analysis; (*iii*) if data gaps were less than 6 h in length, linear interpolation was used to estimated the missing data; (*iv*) any day which, after interpolation, did not have a complete diurnal cycle (i.e., 48 half-hourly values) of the necessary measurements for estimation (air temperature, humidity, friction velocity, net incoming solar radiation, incoming longwave radiation, and ground heat flux) was not used in the analysis.

ACKNOWLEDGMENTS. We thank the AmeriFlux primary investigators of the sites in this study whose work made this research possible: Tilden Meyers (Audubon Research Ranch, Fort Peck), Ram Oren (Duke Forest), Sashi Verma (Mead Rainfed), and Dennis Baldocchi (Vaira and Tonzi Ranch).

1. Priestley CH, Taylor RJ (1972) Assessment of surface heat flux and evaporation using large scale parameters. *Mon Weather Rev* 100(2):81–92.
2. Raupach MR (2001) Combination theory and equilibrium evaporation. *Q J R Metereol Soc* 127:1149–1181.
3. Eichinger W, Parlange MB, Stricker H (1996) On the concept of equilibrium evaporation and the value of the Priestley-Taylor coefficient. *Water Resour Res* 32(1):161–164.
4. Bouchet RJ (1963) Evapotranspiration réelle evapotranspiration potentielle, signification climatique. *Proc Int Assoc Sci Hydrol* 62:134–142.
5. Morton FI (1969) Potential evaporation as a manifestation of regional evaporation. *Water Resour Res* 5(6):1244–1255.
6. Kahler DM, Brutsaert W (2006) Complementary relationship between daily evaporation in the environment and pan evaporation. *Water Resour Res* 42(5):W05413, 10.1029/2005WR004541.
7. Pettijohn JC, Salvucci GD (2005) A new two-dimensional physical basis for the complementary relation between terrestrial and pan evaporation. *J Hydrometeorol* 10(2): 565–574.
8. Fisher JB, Tu KP, Baldocchi DD (2008) Global estimates of the land-atmosphere water flux based on monthly AVHRR and ISLSCP-II data, validated at 16 FLUXNET sites. *Remote Sens Environ* 112(3):901–919.
9. Wang J, Salvucci GD, Bras RL (2004) An extremum principle of evaporation. *Water Resour Res* 40(9):W09303, 10.1029/2004WR003087.
10. Wang J, Bras RL (2011) A model of evapotranspiration based on the theory of maximum entropy production. *Water Resour Res* 47(3):W03521, 10.1029/2010WR009392.
11. Kleidon A, Schymanski S (2008) Thermodynamics and optimality of the water budget on land. *Geophys Res Lett* 35(20):L20404, 10.1029/2008GL035393.
12. Wang KC, Dickinson RE (2012) A review of global terrestrial evapotranspiration: observation, modeling, climatology, and climatic variability. *Rev Geophys* 50(2): RG2005, 10.1029/2011RG000373.
13. Garratt JR (1994) *The Atmospheric Boundary Layer* (Cambridge Univ Press, New York), 1st Paperback Ed (with corrections).
14. AmeriFlux, AmeriFlux Data Products and Access. Available at http://public.ornl.gov/ameriflux/dataproducts.shtml. Accessed April 19, 2012.
15. Gentine P, Polcher J, Entekhabi D (2011) Harmonic propagation of variability in surface energy balance within a coupled soil-atmosphere system. *Water Resour Res* 47(5)(W05525):21, 10.1029/2010WR009268.
16. Groisman PY, et al. (2004) Contemporary changes of the hydrological cycle over the contiguous united states: trends derived from in situ observations. *J Hydrometeorol* 5(1):64–85.
17. Milly PCD, Dunne KA, Vecchia AV (2005) Global pattern of trends in streamflow and water availability in a changing climate. *Nature* 438(7066):347–350.
18. Brutsaert W (2005) *Hydrology, an Introduction* (Cambridge Univ Press, New York).
19. Abramowitz G, Pouyanné L, Ajami H (2012) On the information content of surface meteorology for downward atmospheric long-wave radiation synthesis. *Geophys Res Lett* 39(4):L04808, 10.1029/2011GL050726.
20. Brutsaert W (1982) *Evaporation into the Amosphere* (Reidel, Dordrecht, The Netherlands).